Fault zone restrengthening and frictional healing: The role of pressure solution

Hideaki Yasuhara
Department of Energy and Geo-Environmental Engineering, Pennsylvania State University, University Park, Pennsylvania, USA

Chris Marone
Department of Geosciences, Pennsylvania State University, University Park, Pennsylvania, USA

Derek Elsworth
Department of Energy and Geo-Environmental Engineering, Pennsylvania State University, University Park, Pennsylvania, USA

Received 15 July 2004; revised 3 February 2005; accepted 17 March 2005; published 24 June 2005.

[1] Laboratory and field observations note the significant role of strength recovery (healing) on faults during interseismic periods and implicate pressure solution as a plausible mechanism. Plausible rates for pressure solution to activate, and the magnitudes of ultimate strength gain, are examined through slide-hold-slide experiments using simulated quartz gouge. Experiments are conducted on fine-grained (110 μm) granular silica gouge, saturated with deionized water, confined under constant normal stress of 5 MPa and at modest temperatures of 20 and 65°C, and sheared at a maximum rate of 20 μm/s. Data at 20°C show a log linear relation between strength gain and the duration of holding periods, whereas the higher temperature observations indicate higher healing rates than the log linear dependencies; these are apparent for hold times greater than ~1000 s. This behavior is attributed to the growth and welding of grain contact areas, mediated by pressure solution. The physical dependencies of this behavior are investigated through a mechanistic model incorporating the serial processes of grain contact dissolution, grain boundary diffusion, and precipitation at the rim of contacts. We use the model to predict strength gain for arbitrary conditions of mean stress, fluid pressure, and temperature. The strength gain predicted under the experimental conditions (σ_{eff} = 5 MPa and T = 65°C) underestimates experimental measurements for hold periods of less than ~1000 s where other frictional mechanisms contribute to strength gain. Beyond this threshold, laboratory observations resemble the trend in the prediction by our mechanistic model, implicating that pressure solution is likely the dominant mechanism for strength gain. The model is applied to the long-term prediction of healing behavior in quartzite fault zones. Predictions show that both rates and magnitudes of gain in contact area increase with an increase in applied stresses and temperatures and that fault healing aided by pressure solution should reach completion within recurrence interval durations ranging from <1 to ~10^4 years, depending on applied stresses, temperatures, and reaction rates.

Citation: Yasuhara, H., C. Marone, and D. Elsworth (2005), Fault zone restrengthening and frictional healing: The role of pressure solution, *J. Geophys. Res.*, *110*, B06310, doi:10.1029/2004JB003327.

1. Introduction

[2] Significant strength recovery is apparent both on faults, observed between earthquakes [*Tadokoro and Ando*, 2002; *Li et al.*, 2003], and in experimental measurements [*Dieterich*, 1972; *Marone*, 1998a; *Olsen et al.*, 1998; *Bos and Spiers*, 2002] at reduced spatial scale. Fault strengthening (healing) exerts significant influence on fault behavior, as evidenced through earthquake nucleation and recurrence, and this time-dependent fault strengthening is well explained by empirical rate- and state-dependent friction laws [*Dieterich*, 1979; *Ruina*, 1983]. However, the precise mechanism of this process remains ill constrained. The importance of fluids in fault zones is apparent (see, e.g., *Hickman et al.* [1995] for a review), and fluids play not only mechanical (i.e., reduction of mean effective stress within faults induced by fluid overpressurization), but also chemical (i.e., densification/lithification and cementation of fault gouge driven by chemical potential gradients) roles in faulting phenomena. The mechanical and chemical effects are complexly coupled,

0148-0227/05/2004JB003327$09.00

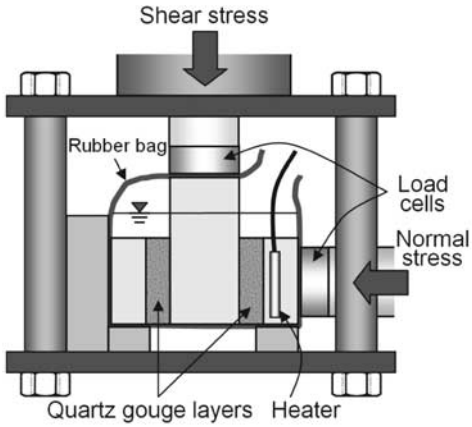

Figure 1. Schematic of the double-direct shear apparatus. Quartz gouge layers are sheared between rough steel blocks. Normal and shear stresses are servo-controlled via two independent actuators. The sample is submerged within deionized water and is heated up to a prescribed temperature (65°C).

and a detailed understanding of the interaction between them is required to define fault healing processes.

[3] Pressure solution [*Weyl*, 1959; *Coble*, 1963; *Rutter*, 1976; *Robin*, 1978; *Raj*, 1982], controlled by gradients of chemical potential, involves three linked processes of dissolution at the stressed interfaces of grain contacts, diffusive transport of dissolved mass from the interface to the pore space, and finally precipitation at the less stressed surface of the grains. This process results in compaction (i.e., reduction in porosity and fluid permeability) and growth and welding of the grain contact areas, and may contribute to strength recovery (healing) on faults during interseismic periods [e.g., *Olsen et al.*, 1998; *Bos and Spiers*, 2002; *Frye and Marone*, 2002]. Alternatively, the progress of pressure solution in hydraulically sealed fault systems may weaken the fault by reducing effective stresses through the augmentation of fluid overpressures [e.g., *Angevine et al.*, 1982]. Pressure solution–aided fault healing is therefore the result of a competition between strengthening and weakening effects; however, the underlying physicochemical mechanisms involved are poorly understood.

[4] Neck growth [*Hickman and Evans*, 1991, 1992] is another conceivable candidate for fault restrengthening. This process is driven by the reduction of interfacial energy and results in the growth of intergranular contact (or neck) area by solute reprecipitation with no time-dependent compaction within faults, and contributing to a concurrent augmentation of shear resistance. Both pressure solution and neck growth may enable the contacting asperities within a fault to be cemented and strengthened, but these processes are driven by different driving forces; the former by mechanical stresses, and the latter by a reduction in interfacial area. Neck growth may dominate when interstitial pore fluids are presaturated with solute and stresses are low, and pressure solution may dominate where intergranular stresses are high; the latter condition is representative of these experiments.

[5] This work examines the effects of fluid-assisted processes (i.e., pressure solution and/or neck growth) on the evolution of strength in simulated fault gouge by conducting slide-hold-slide friction experiments at low temperatures in the range 20 to 65°C. These time- and temperature-dependent observations are explained through a model representing the growth in contact area that evolves between contacting grains as a result of pressure solution [*Yasuhara et al.*, 2003]. Model predictions are compared with experimental measurements of changes in frictional strength as a function of hold periods. Subsequently, the model is extended to investigate the contribution of pressure solution to fault healing in natural faults by simulating environmental conditions for an extended range of applied stresses and temperatures.

2. Experimental Method

[6] A series of slide-hold-slide (SHS) friction experiments was conducted within a double-direct shear testing apparatus (for details, see *Marone* [1998a] and *Karner and Marone* [2000]). A constant normal load was maintained by servo control in feedback mode with 0.1 kN resolution, with shear loads applied by displacement servo control with 0.1 μm resolution. Loads and displacements in both the vertical and horizontal directions were measured and controlled by load cells and displacement transducers, respectively.

2.1. Material

[7] Test samples comprised 3-mm thick layers of quartz powder, which were sheared between rough steel forcing blocks. Grooves were machined perpendicular to the shear direction to eliminate slip at the layer boundaries and confine shear within the granular layers. The area sheared was constant at 10×10 cm^2. The quartz powder was subangular Ottawa sand (>99% of SiO_2) as supplied by the U.S. Silica. Co. We used Natural Grain Product F-110, which has an initial median particle size of 110 μm and a size range of 50–150 μm. Gouge layers were constructed in a leveling jig to ensure that layers were uniform and reproducible at 3.0 mm thick. Sample preparation and experimental procedures are documented in detail by *Frye and Marone* [2002].

2.2. Experimental Procedure

[8] Mounted in the loading system, the three-block sample was shrouded with a thin rubber membrane (see Figure 1), and the normal stress, σ_n, was incremented to 40 MPa. Once stressed, the sample and three-block assemblage were submerged within deionized water.

[9] Subsequently, two tests of p217 and p219 were conducted at temperatures of 20 and 65°C (±1.5°C), respectively. Heating was accomplished by twin thin cylindrical electrical resistance heaters, submerged within the water bath, with convective heat transfer augmented by a submerged air pump. Thermocouples maintained the water bath and sample at the prescribed temperature, which was elevated to 65°C at a rate of ~0.3°C/min while the normal stress of 40 MPa was maintained constant.

[10] Prior to beginning the SHS tests at 20 and 65°C, the gouge layers were precompacted by performing three shear load cycles at 40 MPa normal stress. Normal stress was then reduced to 25 MPa and the gouge layers were sheared to a

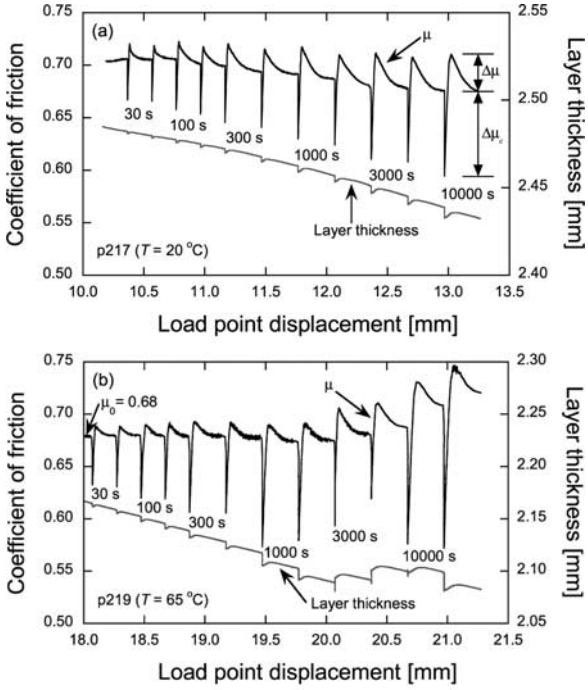

Figure 2. Coefficient of friction (black line) and layer thickness (gray line) are plotted versus load point displacement (a) at 20°C and (b) at 65°C. Both experiments show clear frictional creep ($\Delta\mu_c$) and frictional healing ($\Delta\mu$).

total offset of 6.5 mm. This procedure was conducted to enhance grain crashing, produce new surface area, and establish a steady state friction level (detailed by *Frye and Marone* [2002]). Finally, normal stress was reduced to 5 MPa and SHS tests were conducted. The normal stress and the shearing rate prescribed during sliding were constant in all experiments at 5 MPa and 20 μm/s, respectively. The effect of hold time on fault strength was examined by conducting SHS tests with hold periods of $30-10^4$ s.

[11] We focused on a chemically simple system (SiO_2 + H_2O) for two reasons. The first is because solution transfer effects can be predicted on the basis of compaction and healing data obtained at higher temperature, though the rates may be very slow in the present tests. The second is that dissolution occurs with no change in pH, making the system transparent to interpretation. The elevated temperature (65°C) in our experiments is significantly lower than those of previous experiments focused in friction behavior on healing (230–927°C) [*Fredrich and Evans*, 1992; *Chester and Higgs*, 1992; *Chester*, 1994; *Karner et al.*, 1997; *Olsen et al.*, 1998; *Tenthorey et al.*, 2003], and in compaction behavior preferably driven by pressure solution (200–600°C) [e.g., *Dewers and Hajash*, 1995; *Niemeijer et al.*, 2002; *Spiers et al.*, 2004]. Pressure solution is rate controlled by temperature, applied stress, and grain size. The dependency on stress and grain size is roughly linear, while the dependency on temperature is of Arrhenius-type (exponential) [e.g., *Yasuhara et al.*, 2003]. Thus even the relatively low temperature (65°C) used in these experiments likely exerts a measurable influence on fault strength recovery (healing) over the effects at room temperature.

3. Experimental Results and Analyses

3.1. Results

[12] SHS tests were conducted to examine the time-dependent frictional restrengthening of simulated fault gouge, mediated by fluid-assisted processes. During the tests, loading and steady frictional sliding was interrupted for periods of $30-10^4$ s, before loading was resumed at the original rate (20 μm/s). Figure 2 shows the changes in both layer thickness and the coefficient of friction, defined as the measured shear stress divided by the applied normal stress (τ/σ_n), as a function of load point displacement at the temperatures of 20 and 65°C. SHS tests conducted at 20°C show the usual monotonic increase of $\Delta\mu_c$, defined as the difference between minimum and steady state sliding friction, and $\Delta\mu$, defined as the difference between peak and steady state sliding friction, with an increase of hold time. Also consistent with prior results is the progress of compaction during shear. For measurements at 65°C, no trend in $\Delta\mu_c$ and $\Delta\mu$ are apparent prior to the limiting hold of 3000 s. Following this, comparable response to the experiment at 20°C is apparent; stable sliding friction (μ_{ss}) systematically increases with an increase of hold time, and posthold dilation dominates over prehold compaction.

[13] Figure 3a shows the change in $\Delta\mu_c$ for hold times between 30 and 10^4 s, at temperatures of 20 and 65°C. Data measured at 20 and 65°C exhibit an increase in $\Delta\mu_c$ with increase in hold time, although both the magnitude and growth rate of $\Delta\mu_c$ at 65°C are slightly greater than at 20°C. However, at 65°C the mismatch between the data and the regression line is observed for hold periods greater than 1000 s.

[14] Figure 3b shows changes in $\Delta\mu$ with log hold time. At 20°C $\Delta\mu$ increased systematically and linearly at a rate of 0.0082 per decade with log hold time, consistent with results from other SHS tests conducted under similar conditions [e.g., *Chester*, 1994; *Frye and Marone*, 2002]. Our results, for saturated materials, indicate a distinct transition in frictional healing at 65°C for hold times greater than 1000 s. We observe a sixfold increase in the healing rate from 0.0041 to 0.026 per decade. This transition documents the significant impact of fluid-assisted processes at elevated temperatures on frictional restrengthening.

[15] We note significant differences between prehold and posthold stable sliding friction ($\Delta\mu_{ss} = \mu_{ss}^{post} - \mu_{ss}^{pre}$) as a function of hold time (Figure 3c). Negative values of $\Delta\mu_{ss}$ denote frictional weakening, and positive values frictional strengthening. The negative and uncorrelated magnitudes of $\Delta\mu_{ss}$ at 20°C indicate that the shearing behavior is predominantly frictionally weakening with little effect of hold time. Conversely, at 65°C, the data show a strong positive trend in frictional strengthening for hold times in excess of 1000 s, clarifying the transition observed in changes in $\Delta\mu$ following this threshold hold time (Figure 3b).

3.2. Analyses

[16] Our experimental measurements (Figure 3) indicate that frictional strengthening is dependent on both heal periods and temperature. This behavior is apparent for hold

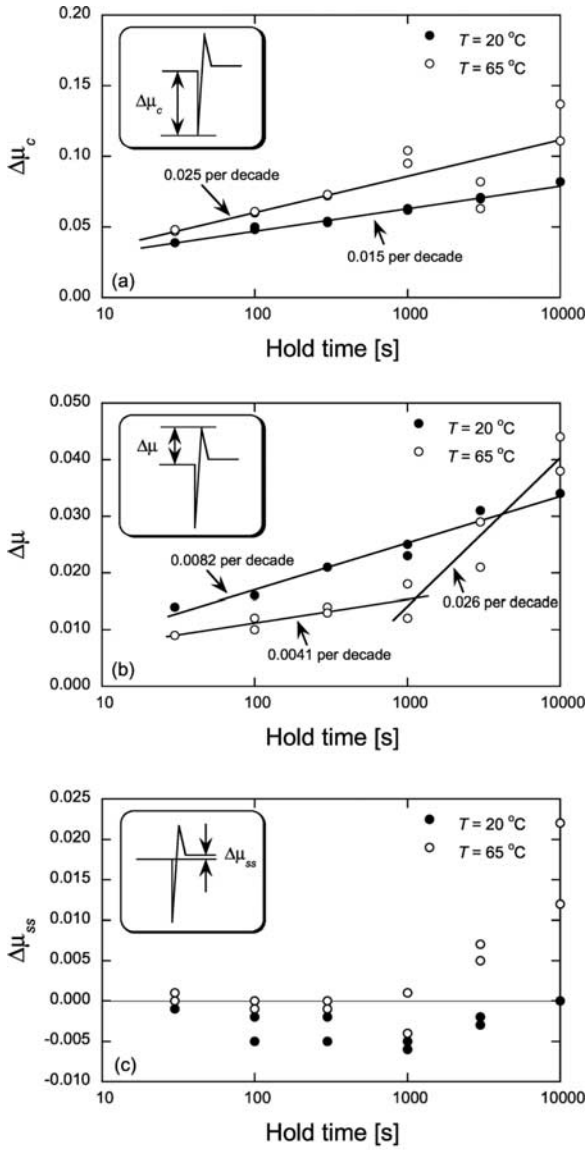

Figure 3. Friction data for $T = 20$ (solid circles) and 65°C (open circles): (a) $\Delta\mu_c$, (b) $\Delta\mu$, and (c) changes in steady state friction ($\Delta\mu_{ss}$) plotted against log hold time. The log linear regression lines are evaluated for $\Delta\mu_c$ and $\Delta\mu$. At 65°C, a distinct transition of $\Delta\mu$ is observed between 1000 and 3000 s hold periods.

periods in excess of 1000 s and at temperatures elevated to 65°C, as evidenced by the prominent transition in the data. The frictional strengthening is attributed to the increase in contact area and/or contact bonding within grains, and may result from the combined effects of frictional processes (i.e., the strengthening of asperities that oppose shear between contact surfaces [*Dieterich*, 1972], which shows a log linear relation between strength gain and the duration of holding periods and is observed typically at room temperature) and the augmentation in cohesion (i.e., strengthening of welded contacts) [*Tenthorey et al.*, 2003; *Muhuri et al.*, 2003]. Of these, the mechanism of the former remains ill constrained, but the latter likely results from pressure solution – a systematic combination of stress-induced mass dissolution at grain contacts (grain indentation), diffusive mass transfer along the grain boundary, and reprecipitation of this mass on the less stressed pore walls (grain cementation) and/or neck growth – a precipitation-dominant process driven by interfacial energy reduction. The effects of pressure solution (i.e., grain cementation resulting in cohesion gain) are observed in gouge microstructures [*Olsen et al.*, 1998; *Kanagawa et al.*, 2000; *Bos et al.*, 2000; *Bos and Spiers*, 2002], and neck growth is reported in the halite/halite lens experiments of *Hickman and Evans* [1991, 1992]. In the halite/halite dissolution experiments, neck growth is observed with no time-dependent convergence (or compaction), whereas in halite/fused-silica experiment, no neck growth occurs with measured convergence, implicating that neck growth is likely a minor contributor to the observed increase in cohesion in our experiments. This follows because during hold periods we observed time-dependent compaction of gouge layers. This interpretation may be further justified from a thermodynamic standpoint. The chemical potential difference $\Delta\mu$ between the stressed contact area and the free face of grains is defined as [e.g., *Heidug*, 1995]

$$\Delta\mu = \sigma_a V_m + \Delta f - 2H\gamma \cdot V_m, \tag{1}$$

where σ_a is the disjoining pressure equal to the amount by which the pressure acting at contact area exceeds the hydrostatic pore pressure, V_m is the molar volume of the solid, Δf is the molar Helmholtz free energy (i.e., elastic and plastic strain energy) difference between the contact and the free pore walls, H is the mean local curvature of the solid-liquid interface, and γ is the specific interfacial energy. The chemical potential difference is the driving force to activate mineral dissolution at the interfacial contact area as compaction (i.e., pressure solution, microcracking, and dislocation creep) proceeds. On the other hand, the effects of applied stress and strain energy (first and second terms in the right-hand side of equation (1)) may be dominated by the effect of interfacial energy as no compaction occurs. If this is the case, the negative chemical potential difference will likely trigger a switching from mineral dissolution (mass export) to precipitation (mass import) around the periphery of the contact area (i.e., neck growth). It is apparent in our experiments that the effect of compaction is dominant, and thus the gain in cohesion observed during hold periods is therefore considered to result mainly from pressure solution.

[17] Although deconvolving the relative contributions of asperity strengthening and grain cementation to the resulting frictional strength, may be difficult, the characteristic transition of frictional gain at 65°C and hold times >1000 s (Figure 3) may be attributed to the switching of the dominance from strengthening of asperities to an increase in cohesion by cementation due to pressure solution. Thus, as an end-member, we analyze frictional strengthening by considering a Coulomb failure criterion ($\tau = c + \sigma_n \mu$), where the microscopic coefficient of friction is assumed constant. An alternate approach would be to account for time-dependent asperity strengthening, based on room temperature measurements, and attribute additional restrengthening to cohesion; however we focus only on the simpler approach, e.g., constant friction, in this paper.

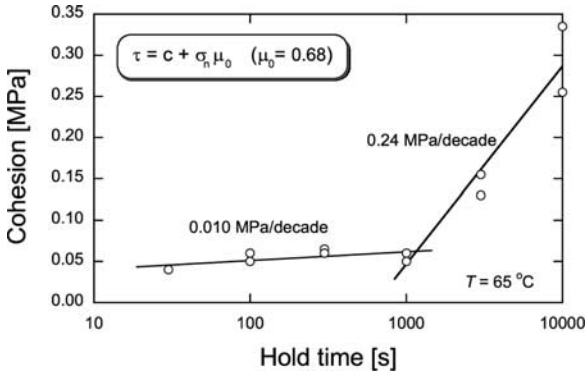

Figure 4. Augmentation in cohesion with log hold time. The rate of increase in cohesion exhibits a rapid increase after 1000 s holding. This transition may result from the active pressure solution, the bonding and growing of contact area, and the cementation by reprecipitation.

[18] Figure 4 shows the augmentation in cohesion with log hold time. The initial cohesion and coefficient of friction are assumed to be zero and 0.68, respectively (μ_0 of 0.68 was obtained from stable sliding friction before the initiation of hold periods (see Figure 2b)). The cohesive contribution to the observed frictional behavior is evaluated by subtracting the effect of friction from the observed shear strength (τ). The frictional component is the product of applied normal stress (5 MPa) and constant coefficient of friction (0.68). The evaluated contribution of cohesion increases at a rate of 0.010 MPa/decade for hold periods of between 30 and 1000 s, followed by a rapid increase in the cohesive strengthening rate of 0.24 MPa/decade, after 1000 s. This further illustrates the growing dominance of cohesive resistance for prolonged hold times, and is consistent with strength augmentation mediated by pressure solution, as opposed to strengthening resulting from asperity strengthening.

[19] This interpretation of the growth in cohesive strengthening with prolonged hold time is supported by the measurements of the change in layer thickness between preholding and postholding and stable sliding friction modes. Figure 5 shows changes in normal strain measured

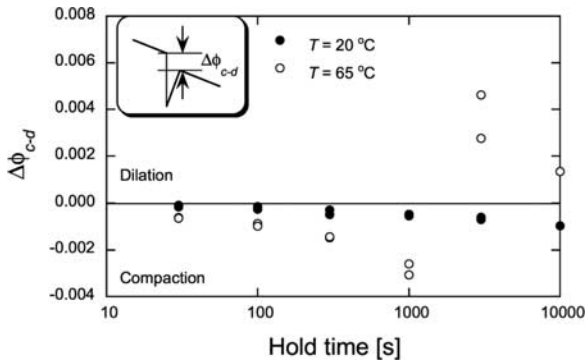

Figure 5. Changes in normal strain between prehealing and posthealing with log hold time. Data at 65°C show that net dilation arises for hold times greater than 3000 s, which likely results from increase of resistance for shearing due to welded grains.

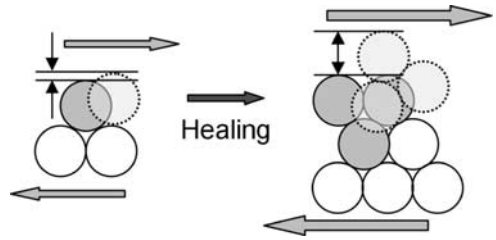

Figure 6. Schematic illustration of behavior of welded grains. The aggregate of bonded grains requires more shear stress and dilation resulting from augmented cohesion driven by pressure solution.

both prehold and posthold, during the SHS tests. The normal strain, $\Delta\phi_{c-d}$, represents the difference between compaction that occurs during heal time, and the peak dilation that occurs immediately after reshear (compaction is denoted negative). Data at 20°C show slight net compaction for all healing times, whereas the higher-temperature measurements indicate net dilation for hold times greater than 3000 s. This response is interpreted to result from the increase in dilation that results when aggregates of welded grains are forced to displace as an assemblage; the welding results from cementation driven by pressure solution. The bonded grain aggregates preferentially dilate upon reshearing, as illustrated in Figure 6, and enhanced dilation mediated by an increase in cohesion contribute to increased frictional strength.

[20] Consistent with this interpretation, $\Delta\mu_{ss}$ is dilational at 65°C for hold times of 3000 and 10000 s (Figure 3c), resulting in a net increase in stable sliding friction. Shearing within a gouge layer is likely localized and an indurated layer (i.e., grain bonded) at the shearing zone result in higher sliding frictional resistance.

4. Quantification of Strength Gain Mediated by Pressure Solution

[21] Data at 65°C show significant augmentation in strength for hold times in excess of 1000 s (Figures 3 and 4). These results reflect the monotonic increase in cohesion with an increase in hold time, and are consistent with the growth of welded grain contacts moderated by solution transfer processes. This interpretation has been suggested as a plausible mechanism for laboratory [e.g., *Karner et al.*, 1997; *Olsen et al.*, 1998; *Bos et al.*, 2000] and field [e.g., *Moore et al.*, 2000; *Tadokoro and Ando*, 2002; *Li et al.*, 2003] observations, yet few relevant theoretical studies examine this process from a mechanistic perspective. In the following we examine time-dependent cohesive strengthening that accompanies the welding of grains by the model of pressure solution for arbitrarily open or closed (hydraulic) systems [*Yasuhara et al.*, 2003]. As noted in the section 3.2, we presume that neck growth exerts little influence on cohesion under our experimental conditions.

4.1. Mechanistic Model

[22] The model of *Yasuhara et al.* [2003] accounts for the three serial processes of grain contact dissolution, grain boundary diffusion, and precipitation at the free grain surface (Figure 7) that prescribe the progress of pressure

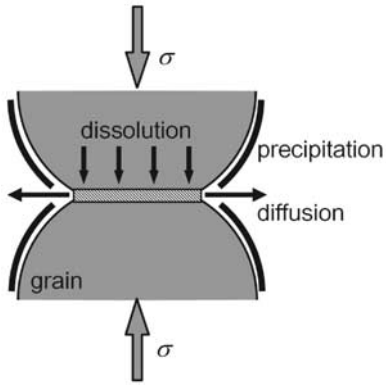

Figure 7. Schematic illustration of pressure solution. This incorporates the serial processes of dissolution at grain-to-grain contacts, interfacial diffusions, and precipitation at the free wall of grain and results in growth and welding of the contact area.

solution. The model procedure allows one to track reaction progress of compaction (i.e., domain shortening and growth of contact area), and pore fluid chemistry, for arbitrary mean stress, fluid pressure, and temperature within both hydraulically open or closed systems. We account for dissolution at the grain-to-grain contacts, mass input to the thin water film between grains [e.g., *Pashley and Kitchener*, 1979; *Tada et al.*, 1987], and mass diffusion along the interface. This mass transport is driven by the gradient in chemical potential between highly stressed contact junctions and less-stressed sites on the pore wall. Supersaturation of the pore fluid solution promotes reprecipitation on the available grain surface. The ensemble processes result in compaction, increased contact area, and possibly augmentation of bonding within asperity contact junctions.

[23] In defining mass redistribution for the serial processes of dissolution, diffusion, and precipitation, it is convenient to utilize the mineral mass fluxes, given by *Yasuhara et al.* [2003] as

$$\frac{dM_{diss}}{dt} = \frac{3\pi V_m^2(\sigma_a - \sigma_c)k_+\rho_g d_c^2}{4RT} \tag{2}$$

$$\frac{dM_{diff}}{dt} = \frac{2\pi\omega D_b}{\ln\left(d_c/2a\right)}\left(C_{int} - C_{pore}\right) \tag{3}$$

$$\frac{dM_{prec}}{dt} = V_p\frac{A}{M}k_-\left(C_{pore} - C_{eq}\right), \tag{4}$$

where dM_{diss}/dt, dM_{diff}/dt, and dM_{prec}/dt represent the dissolution, diffusion, and precipitation mass fluxes, respectively. In equation (2) σ_c is the critical stress, which defines the stress state where the compaction of grain aggregates will effectively halt, k_+ is the dissolution rate constant of the solid, ρ_g is the grain density (2650 kg m^{-3} for quartz), d_c is the diameter of the asperity contact, R is the gas constant, and T is the temperature of the system. In equation (3) ω is the thickness of the water film trapped at the interface, D_b is the diffusion coefficient, a is an infinitesimal length (which we set to one thousandth of the diameter of the initial asperity contact) substituted to avoid a singularity in integrating Fick's first law to the center of a circular contact area, and $(C_{int})_{x=a}$ and $(C_{pore})_{x=d_c}/2$ are mineral concentrations in the interface fluid and pore space, respectively. In equation (4) V_p is the pore volume, k_- is the precipitation rate constant of the dissolved mineral, and C_{eq} is the equilibrium solubility of the dissolved mineral. A is the relative grain surface area, and M is the relative mass of the fluid, which are dimensionless quantities defined by *Rimstidt and Barnes* [1980]. In equation (2) the critical stress, σ_c, is determined by considering the energy balance under applied stress and temperature conditions, given by (see *Revil* [1999] as modified from the work by *Stephenson et al.* [1992]),

$$\sigma_c = \frac{E_m\left(1 - {}^{T}/_{T_m}\right)}{4V_m}, \tag{5}$$

where E_m and T_m are the heat and temperature of fusion, respectively (E_m = 8.57 kJ mol^{-1}, T_m = 1883 K for quartz).

[24] The crucial parameters of dissolution/precipitation rate constant, k_+/k_-, diffusion coefficient, D_b, and equilibrium solubility, C_{eq}, are well constrained for quartz and all have Arrhenius-type dependence with temperature, given by

$$k_+ = k_+^0\exp(-E_{k+}/RT) \tag{6}$$

$$k_- = k_-^0\exp(-E_{k-}/RT) \tag{7}$$

$$D_b = D_0\exp(-E_D/RT) \tag{8}$$

$$C_{eq} = C_0\exp(-E_C/RT). \tag{9}$$

Appropriate magnitudes are selected for these constants defining the temperature dependence as k_+^0 = 1.59 mol m^{2}s^{-1} and E_{k+} = 71.3 kJ mol^{-1} [*Dove and Crerar*, 1990], k_-^0 = 0.196 s^{-1} and E_{k-} = 49.8 kJ mol^{-1} [*Rimstidt and Barnes*, 1980], $D_0 = 5.2 \times 10^{-8}$ m^{2}s^{-1} and E_D = 13.5 kJ mol^{-1} [*Revil*, 1999], and C_0 = 67.6 kg m^{-3} and E_C = 21.7 kJ mol^{-1}.

[25] The solute concentrations that develop, both at the interface between grains, C_{int}, and within the pore fluid, C_{pore}, may be evaluated by considering mass balance within the system [*Yasuhara et al.*, 2003], as

$$\begin{Bmatrix} C_{int} \\ C_{pore} \end{Bmatrix}_{t+\Delta t} = \begin{bmatrix} D_1 + V_p/4\Delta t & -D_1 \\ -D_1 & D_1 + D_2 + V_p/2\Delta t \end{bmatrix}^{-1} \cdot \left[\begin{Bmatrix} dM_{diss}/dt \\ D_2 \cdot C_{eq} \end{Bmatrix}_{t+\Delta t} + \frac{1}{4\Delta t}\begin{bmatrix} V_p & 0 \\ 0 & 2V_p \end{bmatrix}\begin{Bmatrix} C_{int} \\ C_{pore} \end{Bmatrix}_t \right], \tag{10}$$

where

$$D_1 = \frac{2\pi\varpi D_b}{\ln(d_c/2a)}, \quad D_2 = V_p\frac{A}{M}k_-. \tag{11}$$

[26] The three processes of dissolution, diffusion, and precipitation, coupled with the associated change in geom-

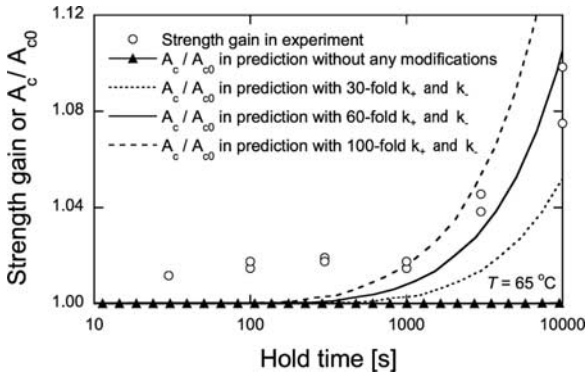

Figure 8. Contrast of the growth of contact area with the evolution of strength observed in the experiments. Strength gain is normalized as the ratio of peak shear stress to the shear strength for initial sliding friction (μ_0 = 0.68). The growth in contact area is normalized relative to the initial Hertzian contact area, A_c/A_{c0}. The predictions underestimate the observed strength gain for hold times less than 1000 s but subsequently follow observations reasonably well, especially for sixtyfold increase.

etry, are combined to define the time-dependent progress of porosity reduction (growth in contact area) and mass concentrations within the interface and pore fluid.

[27] The model initial conditions are established by Hertzian contacts of area, A_{c0}, between hemispherical grains, given by

$$A_{c0} = \frac{\pi\, d^2}{4}\left(\frac{3\,\sigma_{eff}\,\pi\,(1-\nu^2)}{4\,E}\right)^{\frac{2}{3}}, \qquad (12)$$

where d is grain diameter, σ_{eff} is mean effective stress, ν is Poisson's ratio, and E is Young's modulus. The representative pore volume is assumed to be water with an equilibrium concentration of quartz. Thus our initial conditions are such that concentrations of quartz in the interface and pore space are identical to the solubility of quartz, C_{eq}. Once stressed, during time step Δt, the masses mobilized by dissolution, diffusion, and precipitation are evaluated simultaneously from equations (2), (3), and (4), respectively. Physically, the dissolved mass evaluated from equation (2) is supplied to the interface, and domain shortening proceeds as this mass passes along the interface by diffusion. Some portion of the dissolved matter is removed from the interface as it exits into the pore fluid, as defined by equation (3). Depending upon the relative concentration differential between the pore fluid solution and the equilibrium concentration, a portion of the mass removed to the pore fluid is deposited to the grain surface (equation (4)) and the geometry of the grain is correspondingly modified (see Appendix A). As a result, the porosity of the system, together with the contact area is evaluated and updated. Simultaneously, concentrations in the interface and pore fluid are updated utilizing equations (10) and (11). An iterative procedure is accommodated to conduct a consistent calculation until the system reaches an equilibrium state.

4.2. Prediction of Strength Gain

[28] The procedure described above is used to follow the progress of interpenetration and grain contact growth for prescribed mean stress and temperature. As a first-order approximation, we assume that cohesive strength is directly proportional to contact area. Correspondingly, the growth in Coulomb cohesion is proportional to the growth in contact area, and the augmentation in contact area may be evaluated from the progress of pressure solution at the grain-grain contact. Figure 8 compares the growth of surface area with the evolution of strength observed in the experiments. Strength gain is normalized as the ratio of peak shear stress, recorded at designated hold times, to the shear strength for initial sliding friction (μ_0 = 0.68). The growth in contact area is normalized relative to the initial Hertzian contact area, A_c/A_{c0} with predictions completed at 65°C for the material parameters summarized in Table 1. Tabulated dissolution and precipitation rate constants (k_+ and k_-), which are the crucial parameters controlling the rate of reaction, are increased thirtyfold, sixtyfold, and hundredfold to assess the magnitude of strength gain in the experimental measurements. These multipliers are relatively large, but are justified by consideration of the larger (but unmeasured) true microscopic reaction area at the grain-grain contact, relative to the macroscopic contact area, A_c, used in the analysis [e.g., *Canals and Meunier*, 1995]. The ratio of the true surface area over the apparent (smooth) surface area may be as high as 20 [*Murphy and Helgeson*, 1989], and the modifications in the reaction rates in the range thirtyfold to one hundredfold remain plausible. Also, shear stresses relax during hold times, and likely results in enhancement in the chemical potential at grain-to-grain contacts (see equation (1)). Enhanced chemical potential would lead to further augmentation in rate of pressure solution, but the model does not account for this effect. This may be another contributor to the underestimation of the observed strength gain, relative to theoretical predictions. As apparent in Figure 8, the predictions underestimate the observed strength gain for hold times less than 1000 s, but subsequently represent observations reasonably well (specifically for the sixtyfold increase). The underpredictions for short hold times are consistent with the minimal influence that pressure solution exerts in this range of the parameter space, relative to other effects (e.g., "frictional healing."). However, once activated, a mechanism of pressure solution healing (i.e., growth and welding/cementing of the contact areas) is consistent with the observed data, with this effect dominating over others for hold times longer than ~1000–3000 s. The predicted transition of the dominant strengthening mechanism from frictional to cohesive (pressure solution) at around 1000 s is also consistent with observations (Figures 3–5).

Table 1. Parameters Utilized in Calculations

Parameter	Value
Diameter d, μm	110
Temperature T, °C	65
Effective Stress σ_{eff}, MPa	5.0
Poisson's Ratio ν	0.3
Young's Modulus E, GPa	70
Critical Stress σ_c, MPa	77.4
Diffusion Path Width ω, nm	4.0
Diffusion Coefficient D_b, m^2s^{-1}	4.27×10^{-10}
Dissolution Rate Constant k_+, mol m^{-2} s^{-1}	1.54×10^{-11}
Precipitation Rate Constant k_-, s^{-1}	3.97×10^{-9}
Solubility of Quartz C_{eq}, ppm	30

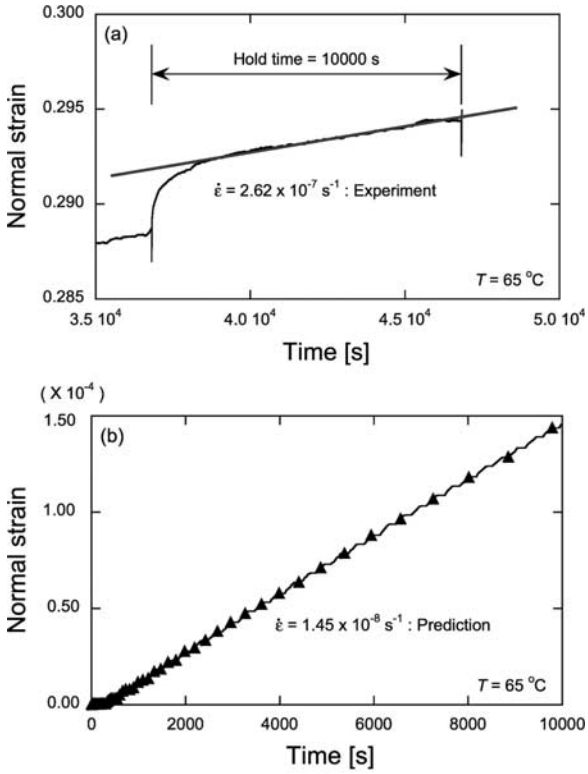

Figure 9. Changes in normal strain (compaction is taken as positive) during healing period for (a) experiment and (b) prediction at 65°C. Strain rates of the observation and the prediction are 2.62×10^{-7} and 1.45×10^{-8} s^{-1}, respectively.

[29] The model is also able to consistently predict magnitudes and rates of compaction during periods of healing. Figure 9 shows changes in both measured and predicted (the sixtyfold increases in k_+ and k_-) normal strain (compaction here is taken as positive) at 65°C. The experimentally observed strain rate recorded during a hold of 10000s duration is 2.62×10^{-7} s^{-1}, and this compares with a predicted magnitude roughly one order of magnitude smaller (1.45×10^{-8} s^{-1}). This underprediction may result from the unaccounted contributions of grain rotations and redistribution (packing densification) and the increase in compaction rate mediated by shear stress.

4.3. Implications for Strength Recovery in Natural Faults

[30] Both the experimental measurements and the model predictions indicate that a quartzitic fault gouge may be indurated by pressure solution processes, and that the log linear relation between healing and waiting period, for example, as predicted by rate and state friction [*Marone*, 1998a], may need to be modified. Notably, the rates of strength recovery based on the log linear relation may significantly underestimate the actual rates and magnitudes of fault healing during long interseismic periods. Although seismic estimates of fault healing appear to be consistent with log linear laboratory values [*Marone et al.*, 1995; *Marone*, 1998b], our data indicate that a quantitative understanding of healing rates in natural fault gouge must account for pressure solution processes and time-dependent evolution of contact area. Neck growth at contacting asperities may be another solution transfer process that strengthens faults during interseismic periods, although this is a minor effect in our experiments. This process may dominate over the effect of pressure solution when effective stresses acting on an enlarged contact area drop sufficiently that pressure solution effectively ceases; this transition will be heralded by an arrest in compaction. However, the interaction between pressure solution and neck growth is still ill constrained, and more work is needed to incorporate a linked process of neck growth in the current model. Thus the process of fault strengthening is hereinafter examined by considering only pressure solution.

[31] To account for fault healing by pressure solution processes, we employ the model developed above, where contact junction growth is used to account for strength gain. Calculations are completed for a variety of representative depths within the fault zone. We use an average effective stress gradient (i.e., overburden minus hydrostatic pressure), and geothermal gradient of 12 MPa/km, and 25°C/km, respectively. Parameters of critical stress, σ_c, dissolution/precipitation rate constants, k_+/k_-, diffusion coefficient, D_b, solubility of quartz, C_{eq}, and Hertzian contact area, A_0, are calculated according to prescribed stress and temperature conditions by equations (5)–(9), and (12), respectively. At all depths an initial grain diameter, d, is set to 110 μm, and a constant water film thickness, ω, of 4.0 nm is assumed, although this thickness may be a function of applied stress [*Pashley*, 1982; *Horn et al.*, 1989]. Figure 10 shows the evolution of contact area with healing time at depths from 1 to 5 km, predicted with both no modifications for all parameters obtained by equations (5)–(9) and (12) and hundredfold increases in the reaction rate constants (k_+ and k_-). Reaction rate constants are well constrained under laboratory environments, but may be scale dependent and the discrepancy

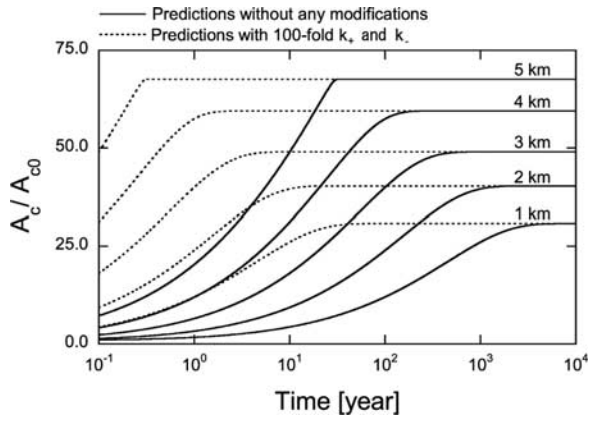

Figure 10. Evolution in contact area, normalized by initial contact area, with healing time at depths from 1 to 5 km. Solid and dotted lines represent predictions without any modifications and with hundredfold increases in reaction rate constants (k_+ and k_-), respectively. Healing rates and magnitudes increase with depth (i.e., applied temperatures and stresses).

between laboratory and filed is poorly understood. The multiplier applied here is relatively large and may be an upper bound for reaction (healing) rates (maybe, even if the effect of neck growth is involved). As apparent in Figure 10, healing rates are magnified linearly with this multiplier; at a depth of 1 km durations to equilibrium are increased from $\sim 10^4$ to $\sim 10^2$ years.

[32] Predictions without modifications in reaction rate constants indicate that both rates and magnitudes of gain in contact area increase with depth. In particular, healing rates are significantly magnified with depth; healing at a depth of 1 km is completed on the order of 10^4 years, whereas less than 50 years is required at depth of 5 km. Importantly, a maximum strength gain results, with this peak strength is both attained more quickly, and of greater magnitude, with increasing depth. The process of pressure solution is jointly mediated by stress and by temperature, with the rates and ultimate magnitudes of strength gain generally controlled by the environmentally applied temperature and stress conditions, respectively. Moreover, the dependency on stress is roughly linear, with the temperature dependency more pronounced because of the linkage of dissolution rates with its Arrhenius-type (exponential) dependence. The exponential dependence on temperature results in rapid augmentation of healing rates between the depths of 1 km (45°C) and 5 km (145°C). Predictions show healing periods in the wide range <1 to $\sim 10^4$ years, depending on depths and applied reaction rates. Specifically, the reaction rates significantly control overall behavior, which requires that they be carefully examined to obtain more realistic predictions on healing processes.

[33] An important component of the model is the ability to calculate the evolution in porosity during compaction. The magnitudes of the ultimate porosity at depths of 1, 3, and 5 km are evaluated as 0.43, 0.27, and 0.06, respectively. Notably, porosities at depths below 5 km are prominently low, and may result in the overpressuring of pore fluids because of impermeable sealing, depending on the evolution in transport properties of the gouge. However, the conditions of this overpressurization are not evaluated in this work. A quantitative and mechanism-based understanding of the generation of overpressurizing is required because this likely results in fault weakening, which could potentially trigger earthquake nucleation [e.g., *Sleep and Blanpied*, 1992; *Tenthorey et al.*, 2003].

5. Conclusions

[34] Laboratory experiments have been conducted to examine the effects of solution transfer processes on frictional healing in simulated quartz gouge layers. Data at 20°C show a log linear relation between healing and hold periods with the frictional healing rate of 0.0082 per decade. At mildly elevated temperature (65°C), frictional healing is faster than suggested by the log linear dependency for hold times above a threshold of ~1000 s. The temperature and hold time threshold for this strength gain suggests pressure solution as a plausible mechanism, strength gain being related to the growth in grain-grain contacts within the particulate assemblage. The feasibility of this pressure solution mechanism is reinforced by observations of increase in the stable sliding friction and generation in posthold dilation more than compaction during healing.

[35] A mechanistic model [*Yasuhara et al.*, 2003] is applied to examine the growth of contact area with time, linking this observation as a proxy for strength gain observed during periods of healing. This model incorporates the process of pressure solution, representing the three serial processes of grain contact dissolution, grain boundary diffusion, and free-wall precipitation. This enables the evolution of contact area to be followed in time under arbitrary prescribed stress and temperature conditions. The model underestimates experimental measurements of fault healing for short hold durations (less than 1000 s), due to the dominant influence of other frictional mechanisms of strength gain. However, for hold durations longer than ~1000 s, rapid growth in strength with hold time is well represented by a model for pressure solution if the unknown magnitude of microscopic asperity contact area is increased over the nominal macroscopic contact area.

[36] For pressure solution, the prediction for strength gain does not show the same log linear dependence between healing and time, apparent in other frictionally based mechanisms. Thus, if healing is rate controlled by pressure solution, extrapolation by the log linear relation may significantly underestimate actual healing rates in natural faults. The model is applied to the long-term prediction of the behavior of fault healing. Predictions show augmentation of healing in both rates and magnitudes with depth, and indicate that pressure solution may form impermeable fault zones and result in pore fluid overpressurization that likely plays a key role in the rupture of fault zones.

Appendix A: Modification in Grain Geometry

[37] The solid quartz volume, V_s, in the representative elementary volume is obtained by subtracting from the volume of a sphere of diameter, d, the sums of the volumes truncated between the hemispheres and the rectangular domain, and between the contacts of two hemispheres, given by,

$$V_s = -\frac{\pi}{3}d^3 + \pi d_z\left(\frac{d^2}{4} - \frac{d_z^2}{12}\right) + \pi d_0\left(\frac{d^2}{2} - \frac{d_0^2}{6}\right), \qquad \text{(A1)}$$

where d_z and d_0 are the domain height and the initial grain diameter. In particular, the volume truncated by the two hemispheres in contact, V_{rem}, is given by

$$V_{rem} = \frac{\pi}{8}\left(\frac{d_z^3}{3} - d_0^2 d_z + \frac{2}{3}d_0^3\right). \qquad \text{(A2)}$$

In a closed system the volume of the quartz grain must balance the initial volume of the grain minus the amount suspended in the pore fluid, and the solid quartz volume, V_s, is also expressed as

$$V_s = \frac{\pi}{6}d_0^3 - \frac{1}{\rho_g}\sum\left(\left(\frac{dM_{diff}}{dt} - \frac{dM_{prec}}{dt}\right)\cdot \Delta t\right). \qquad \text{(A3)}$$

Since the domain shortening proceeds as the mass dissolved passes along the interface by diffusion, the volume truncated by the two hemispheres in contact is given by

$$V_{rem} = \frac{1}{\rho_g} \sum \left(\frac{dM_{diff}}{dt} \cdot \Delta t \right). \tag{A4}$$

From equations (A1)–(A4) we can obtain the diameter, d, of the modified sphere and the domain height, d_z. Then, using these values, the porosity, ϕ, the cross-sectional area of the modified sphere, A_{mod}, and the diameter of contact area, d_c, are calculated, as

$$\phi = 1 - \frac{V_s}{d_0^2 d_z} \tag{A5}$$

$$A_{mod} = \frac{\pi}{4} d^2 - d^2 \cdot \arccos\left(\frac{d_0}{d}\right) + d_0 \sqrt{d^2 - d_0^2} \tag{A6}$$

$$d_c = \sqrt{d_0^2 - d_z^2} + (d - d_0). \tag{A7}$$

[38] For a uniaxial compaction, the force applied at the quartz aggregate balances the force applied at the contact area, and the stress applied at the contact area, σ_a, is obtained as

$$\sigma_{eff} \cdot A_{mod} = \sigma_a \cdot \frac{\pi}{4} d_c^2 \tag{A8}$$

$$\sigma_a = \sigma_{eff} \cdot \frac{A_{mod}}{\frac{\pi}{4} d_c^2}. \tag{A9}$$

[39] Through this process, the grain geometry is modified at each time step, Δt, and the porosity is updated until the system reaches an equilibrium state when the stress applied at contact area, σ_a, becomes equivalent to the critical stress, σ_c.

[40] **Acknowledgments.** This work is a result of partial support under grants DOE-BES-DE-FG02-00ER15111, (NSF) OCE-0196462, (NSF) EAR-0196570, and DE-FG36-04GO14289. This support is gratefully acknowledged. The authors thank Jennifer Anthony and Amir Polak for help in the experimental portion of the study and Chris Spiers and Teruo Yamashita for insightful review and helpful comments on this manuscript.

References

Angevine, C. L., D. L. Turcotte, and M. D. Furnish (1982), Pressure solution lithification as a mechanism for the stick-slip behavior of faults, *Tectonics*, *1*, 151–160.

Bos, B., and C. J. Spiers (2002), Fluid-assisted healing processes in gouge-bearing faults: Insights from experiments on a rock analogue system, *Pure Appl. Geophys.*, *159*, 2537–2566.

Bos, B., C. J. Peach, and C. J. Spiers (2000), Slip behavior of simulated gouge-bearing faults under conditions favoring pressure solution, *J. Geophys. Res.*, *105*, 16,699–16,717.

Canals, M., and J. D. Meunier (1995), A model for porosity reduction in quartzite reservoirs by quartz cementation, *Geochim. Cosmochim. Acta*, *59*, 699–709.

Chester, F. M. (1994), Effects of temperature on friction: Constitutive equations and experiments with quartz gouge, *J. Geophys. Res.*, *99*, 7247–7261.

Chester, F. M., and N. G. Higgs (1992), Multimechanism friction constitutive model for ultrafine quartz gouge at hypocentral conditions, *J. Geophys. Res.*, *97*, 1859–1870.

Coble, R. L. (1963), A model for boundary diffusion controlled creep in polycrystalline materials, *J. Appl. Phys.*, *34*, 1679–1682.

Dewers, T., and A. Hajash (1995), Rate laws for water-assisted compaction and stress-induced water-rock interaction in sandstones, *J. Geophys. Res.*, *100*, 13,093–13,112.

Dieterich, J. H. (1972), Time-dependent friction in rocks, *J. Geophys. Res.*, *77*, 3690–3697.

Dieterich, J. H. (1979), Modeling of rock friction: 1. Experimental results and constitutive equations, *J. Geophys. Res.*, *84*, 2161–2168.

Dove, P. M., and D. A. Crerar (1990), Kinetics of quartz dissolution in electrolyte solutions using a hydrothermal mixed flow reactor, *Geochim. Cosmochim. Acta*, *54*, 955–969.

Fredrich, J. T., and B. Evans (1992), Strength recovery along simulated faults by solution transfer processes, *Proc. U.S. Rock Mech. Symp.*, *33*, 121–130.

Frye, K. M., and C. Marone (2002), Effect of humidity on granular friction at room temperature, *J. Geophys. Res.*, *107*(B11), 2309, doi:10.1029/2001JB000654.

Heidug, W. K. (1995), Intergranular solid-fluid phase transformations under stress: The effect of surface forces, *J. Geophys. Res.*, *100*, 5931–5940.

Hickman, S. H., and B. Evans (1991), Experimental pressure solution in halite: The effect of grain/interphase boundary structure, *J. Geol. Soc. London*, *148*, 549–560.

Hickman, S. H., and B. Evans (1992), Growth of grain contacts in halite by solution-transfer: Implications for diagenesis, lithification, and strength recovery, in *Fault Mechanics and Transport Properties of Rocks*, edited by B. Evans and T.-F. Wong, pp. 253–280, Elsevier, New York.

Hickman, S., R. Sibson, and R. Bruhn (1995), Introduction to special section: Mechanical involvement of fluids in faulting, *J. Geophys. Res.*, *100*, 12,831–12,840.

Horn, R. G., D. T. Smith, and W. Haller (1989), Surface forces and viscosity of water measured between silica sheets, *Chem. Phys. Lett.*, *162*, 404–408.

Kanagawa, K., S. F. Cox, and S. Zhang (2000), Effects of dissolution-precipitation processes on the strength and mechanical behavior of quartz gouge at high-temperature hydrothermal conditions, *J. Geophys. Res.*, *105*, 11,115–11,126.

Karner, S. L., and C. Marone (2000), Effects of loading rate and normal stress on stress drop and stick-slip recurrence interval, in *Geocomplexity and the Physics of Earthquakes*, *Geophys. Monogr. Ser.*, vol. 120, edited by J. B. Rundle, D. L. Turcotte, and W. Klein, pp. 187–198, AGU, Washington, D. C.

Karner, S. L., C. Marone, and B. Evans (1997), Laboratory study of fault healing and lithification in simulated fault gouge under hydrothermal conditions, *Techtonophysics*, *277*, 41–55.

Li, Y.-G., J. E. Vidale, S. M. Day, D. D. Oglesby, and E. Cochran (2003), Postseismic fault healing on the rupture zone of the 1999 *M* 7.1 Hector Mine, California, earthquake, *Bull. Seismol. Soc. Am.*, *93*, 854–869.

Marone, C. (1998a), Laboratory-derived friction laws and their application to seismic faulting, *Annu. Rev. Earth Planet. Sci.*, *26*, 643–696.

Marone, C. (1998b), The effect of loading rate on static friction and the rate of fault healing during the earthquake cycle, *Nature*, *391*, 69–72.

Marone, C., J. E. Vidale, and W. Ellsworth (1995), Fault healing inferred from time dependent variations in source properties of repeating earthquakes, *Geophys. Res. Lett.*, *22*, 3095–3098.

Moore, D. E., D. A. Lockner, H. Ito, and R. Ikeda (2000), Proceedings of the international workshop on the Nojima fault core and borehole data analysis, *U.S. Geol. Surv. Open File Rep.*, *00–129*, 159–165.

Muhuri, S. K., T. A. Dewers, T. E. Scott Jr., and Z. Reches (2003), Interseismic fault strengthening and earthquake-slip stability: Friction or cohesion?, *Geology*, *31*(10), 881–884.

Murphy, W. M., and H. C. Helgeson (1989), Thermodynamic and kinetic constraints on reaction rates among minerals and aqueous solutions: IV. Retrieval of rate constants and activation parameters for the hydrolysis of pyroxene, wollastonite, olivine, andalusite, quartz, and nepheline, *Am. J. Sci.*, *289*, 17–101.

Niemeijer, A. R., C. J. Spiers, and B. Bos (2002), Compaction creep of quartz sand at 400–600°C: Experimental evidence for dissolution-controlled pressure solution, *Earth Planet. Sci. Lett.*, *195*, 261–275.

Olsen, M. P., C. H. Scholz, and A. Léger (1998), Healing and sealing of a simulated fault gouge under hydrothermal conditions: Implications for fault healing, *J. Geophys. Res.*, *103*, 7421–7430.

Pashley, R. M. (1982), Hydration forces between mica surfaces in electrolyte solutions, *Adv. Colloid Interface Sci.*, *16*, 57–62.

Pashley, R. M., and J. A. Kitchener (1979), Surface forces in adsorbed multilayers of water on quartz, *J. Colloid Interface Sci.*, *71*, 491–500.

Raj, R. (1982), Creep in polycrystalline aggregates by matter transport through a liquid phase, *J. Geophys. Res.*, *87*, 4731–4739.

Revil, A. (1999), Pervasive pressure-solution transfer: A poro-visco-plastic model, *Geophys. Res. Lett.*, *26*, 255–258.

Rimstidt, J. D., and H. L. Barnes (1980), The kinetics of silica-water reactions, *Geochim. Cosmochim. Acta*, *44*, 1683–1699.

Robin, P.-Y. F. (1978), Pressure solution at grain-to-grain contacts, *Geochim. Cosmochim. Acta*, *42*, 1383–1389.

Ruina, A. (1983), Slip instability and state variable friction laws, *J. Geophys. Res.*, *88*, 10,359–10,370.

Rutter, E. H. (1976), The kinetics of rock deformation by pressure solution, *Philos. Trans. R. Soc. London, Ser. A*, *283*, 203–219.

Sleep, N. H., and M. L. Blanpied (1992), Creep, compaction and the weak rheology of major faults, *Nature*, *359*, 687–692.

Spiers, C. J., S. De Meer, A. R. Niemeijer, and X. Zhang (2004), Kinetics of rock deformation by pressure solution and the role of thin aqueous films, in *Physicochemistry of Water in Geological and Biological Systems—Structures and Properties of Thin Aqueous Films*, edited by S. Nakashima et al., pp. 129–158, Universal Acad. Press, Tokyo.

Stephenson, L. P., W. J. Plumley, and V. V. Palciauskas (1992), A model for sandstone compaction by grain interpenetration, *J. Sediment. Petrol.*, *62*, 11–22.

Tada, R., R. Maliva, and R. Siever (1987), Rate laws for water-assisted compaction and stress-induced water-rock interaction in sandstones, *Geochim. Cosmochim. Acta*, *51*, 2295–2301.

Tadokoro, K., and M. Ando (2002), Evidence for rapid fault healing derived from temporal changes in S wave splitting, *Geophys. Res. Lett.*, *29*(4), 1047, doi:10.1029/2001GL013644.

Tenthorey, E., S. F. Cox, and H. F. Todd (2003), Evolution of strength recovery and permeability during fluid-rock reaction in experimental fault zones, *Earth Planet. Sci. Lett.*, *206*, 161–172.

Weyl, P. K. (1959), Pressure solution and force of crystallization: A phenomenological theory, *J. Geophys. Res.*, *64*, 2001–2025.

Yasuhara, H., D. Elsworth, and A. Polak (2003), A mechanistic model for compaction of granular aggregates moderated by pressure solution, *J. Geophys. Res.*, *108*(B11), 2530, doi:10.1029/2003JB002536.

D. Elsworth and H. Yasuhara, Department of Energy and Geo-Environmental Engineering, Pennsylvania State University, University Park, PA 16802, USA. (huy103@psu.edu)

C. Marone, Department of Geosciences, Pennsylvania State University, University Park, PA 16802, USA.